

Accepted Article

Title: Thermal Unequilibrium of PdSn Intermetallic Nanocatalysts:
From in situ Tailored Synthesis to Unexpected Hydrogenation
Selectivity

Authors: Minda Chen, Yu Yan, Mebatsion Gebre, Claudio Ordonez,
Fudong Liu, Long Qi, Andrew Lamkins, Dapeng Jing, Kevin
Dolge, Biying Zhang, Patrick Heintz, Daniel P. Shoemaker,
Bin Wang, and Wenyu Huang

This manuscript has been accepted after peer review and appears as an Accepted Article online prior to editing, proofing, and formal publication of the final Version of Record (VoR). This work is currently citable by using the Digital Object Identifier (DOI) given below. The VoR will be published online in Early View as soon as possible and may be different to this Accepted Article as a result of editing. Readers should obtain the VoR from the journal website shown below when it is published to ensure accuracy of information. The authors are responsible for the content of this Accepted Article.

To be cited as: *Angew. Chem. Int. Ed.* 10.1002/anie.202106515

Link to VoR: <https://doi.org/10.1002/anie.202106515>

RESEARCH ARTICLE

Thermal Unequilibrium of PdSn Intermetallic Nanocatalysts: From *in situ* Tailored Synthesis to Unexpected Hydrogenation Selectivity

Minda Chen, Yu Yan, Mebatsion Gebre, Claudio Ordonez, Fudong Liu, Long Qi, Andrew Lamkins, Dapeng Jing, Kevin Dolge, Biying Zhang, Patrick Heintz, Daniel P. Shoemaker,* Bin Wang,* and Wenyu Huang*

Abstract: Effective control on chemoselectivity in the catalytic hydrogenation of C=O over C=C bonds is uncommon with Pd-based catalysts because of the favored adsorption of C=C bonds on Pd surface. Here we report a unique orthorhombic PdSn intermetallic phase with unprecedented chemoselectivity toward C=O hydrogenation. We observed the formation and metastability of this PdSn phase *in situ*. During a natural cooling process, the PdSn nanoparticles readily revert to the favored Pd₃Sn₂ phase. Instead, using a thermal quenching method, we prepared a pure-phase PdSn nanocatalyst. PdSn shows an >96% selectivity toward hydrogenating C=O bonds of various α,β -unsaturated aldehydes, highest in reported Pd-based catalysts. Further study suggests that efficient quenching prevents the reversion from PdSn- to Pd₃Sn₂-structured surface, the key to the desired catalytic performance. Density functional theory calculations and analysis of reaction kinetics provide an explanation for the observed high selectivity.

Introduction

Chemoselectivity is a keystone of catalysis. In the catalytic hydrogenation reaction, chemoselectivity of C=O bonds over C=C bonds is significant in producing industrial chemicals due to the high demand for unsaturated alcohols in food, pharmaceutical,

fragrance, and other industries. However, thermodynamics naturally favors the hydrogenation of C=C bonds by ca. 35 kJ/mol, making it challenging to improve C=O selectivity.^[1] Many studies in heterogeneous catalysis have been devoted to selective hydrogenation of C=O over C=C bonds, using α,β -unsaturated aldehydes as model substrates. Studies on Pd-based catalysts, however, are limited. Due to the small *d* bandwidth, Pd has a weak repulsive interaction and thus a strong absorption with the C=C group in the α,β -unsaturated aldehyde.^[1] This strong interfacial binding makes Pd the least selective catalyst toward C=O hydrogenation among common transition metals. A generally accepted trend of C=O hydrogenation selectivity is Os > Ir > Pt > Ru > Rh > Pd.^[1b] Pd catalysts are reported to have little or no selectivity to unsaturated alcohol from acrolein, crotonaldehyde, or cinnamaldehyde substrates.^[2] Notably, the structure of reactants is also crucial to the selective hydrogenation of C=O over C=C. On a substrate molecule with less sterically hindered groups in the vicinity of the C=C group, such as acrolein, methacrolein, and crotonaldehyde, it is much more challenging to achieve high selectivity to the C=O hydrogenation.^[1, 3]

The use of bimetallic catalysts is a common strategy to improve the chemoselectivity for C=O hydrogenation.^[4] Previous work in our group demonstrated that a PtSn@SiO₂ catalyst could hydrogenate the C=O group in furfural with >96% selectivity and 40 times higher activity than Pt@SiO₂.^[5] Although Pd-based bimetallic catalysts, such as Pd-Cu,^[6] Pd-Ni^[7], Pd-Zn,^[2a, 8] and Pd-Sn^[9] have been reported to outperform the monometallic Pd catalysts, none of them exhibit dominant selectivity (>50%) for C=O hydrogenation with relatively challenging substrates (acrolein, crotonaldehyde or methacrolein). Even for less challenging substrates, such as cinnamaldehyde, furfural, or citral, the best hydrogenation selectivity for C=O is only ~75%.^[9a]

Pd-based intermetallic nanoparticles (iNPs) are recognized as efficient and selective catalysts, and Pd_xSn_y iNPs are no exception.^[10] With numerous work on Pd-Sn bimetallic catalysts, it is to our surprise that PdSn iNPs with a FeAs-type orthorhombic crystal structure has rarely been reported, while catalysts with a monoclinic Pd₃Sn₂ structure are well discussed.^[11] Schaak et al. reported the synthesis of PdSn iNPs by growing Pd on >20 nm Sn seeds, although their catalytic properties have not been explored.^[12] In this study, we investigated the formation of the orthorhombic PdSn iNPs through *in-situ* powder X-ray diffraction (PXRD) and X-ray absorption spectroscopy (XAS) studies. Unlike the bulk intermetallic phase, PdSn at nanoscale exhibit distinct formation behavior. High-temperature annealing is required for the formation of PdSn phase, which reverts to the thermodynamically favored Pd₃Sn₂ phase during a natural cooling-down process. Using a rapid quenching method, we

[*] M. Chen, C. Ordonez, A. Lamkins, K. Dolge, B. Zhang, P. Heintz, Prof. W. Huang

Department of Chemistry, Iowa State University
Ames, IA 50011, United States

E-mail: whuang@iastate.edu

Y. Yan, Prof. B. Wang

School of Chemical, Biological, and Materials Engineering
The University of Oklahoma

Norman, Oklahoma 73019, United States

E-mail: wang_cbme@ou.edu

M. Gebre, Prof. D. P. Shoemaker

Department of Materials Science and Engineering

University of Illinois Urbana-Champaign

Urbana, IL 61801, United States

E-mail: dpshoema@illinois.edu

Prof. F. Liu

Department of Civil, Environmental, and Construction Engineering
Catalysis Cluster for Renewable Energy and Chemical Transformations

(REACT), NanoScience Technology Center (NSTC)

University of Central Florida

Orlando, FL 32816, United States

Dr. L. Qi, Dr. D. Jing, Prof. W. Huang

Ames Laboratory, U.S. Department of Energy

Ames, IA 50011, United States

Dr. D. Jing

Materials Analysis and Research Laboratory, Iowa State University

Ames, IA 50011, United States

Supporting information for this article is given via a link at the end of the document

RESEARCH ARTICLE

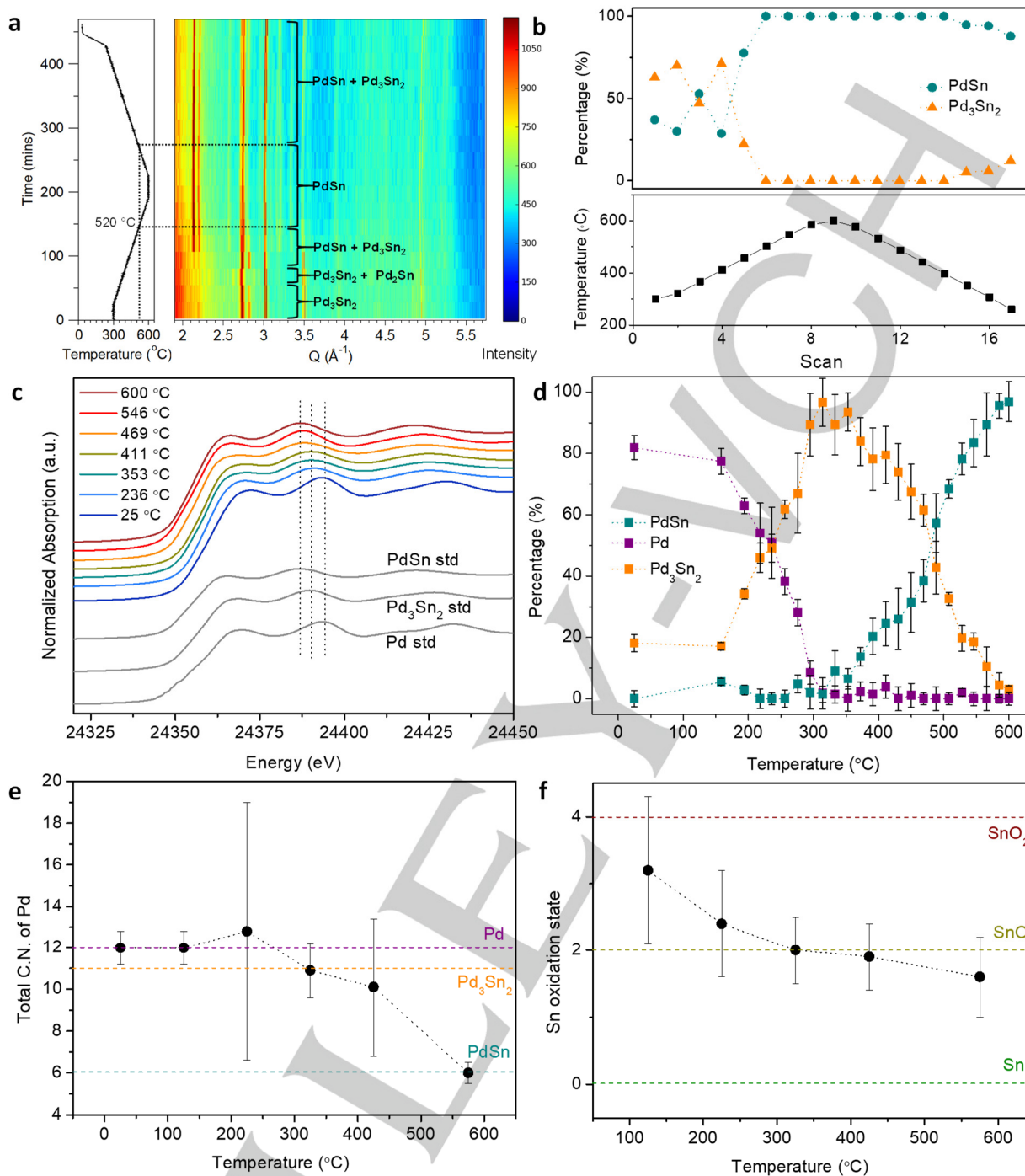


Figure 1. (a) *In-situ* PXRD measurement of the formation of PdSn under a reducing condition from 300 to 600 $^{\circ}\text{C}$. (b). The PdSn and Pd₃Sn₂ components for each scan in (a) quantified by Rietveld analysis. (c) *In-situ* XANES spectra at the Pd K-edge recorded at different temperatures during the phase transition induced by reduction. (d) Linear combination fitting result of the XANES data in (c). (e) The total coordination number of Pd measured from Pd K-edge EXAFS fitting. (f) The oxidation state of Sn measured from linear combination fitting of Sn K-edge XANES spectra.

successfully synthesized the PdSn INPs with high phase purity. In the hydrogenation of a variety of α,β -unsaturated aldehydes, the PdSn INPs are highly selective to hydrogenate C=O bonds, which

is unique among other monometallic/bimetallic catalysts involving Pd. It is also the highest C=O hydrogenation selectivity observed for α,β -unsaturated aldehydes using a Pd-based catalyst.

RESEARCH ARTICLE

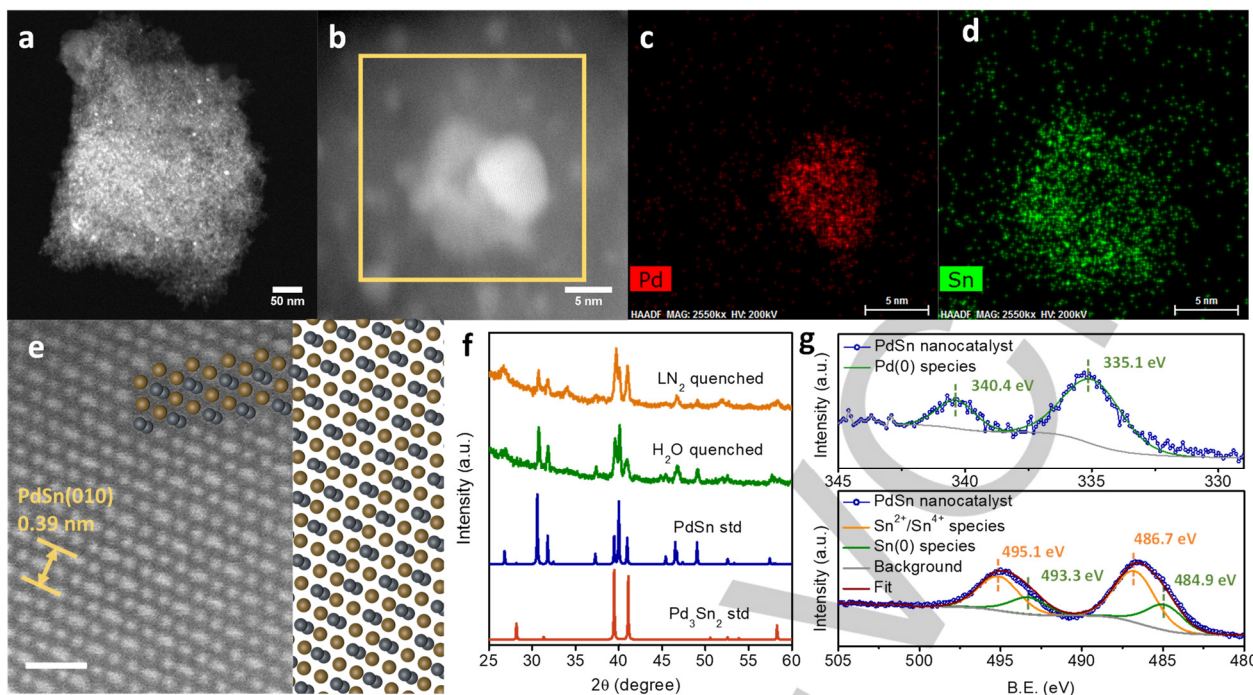


Figure 2. Characterization of the PdSn nanocatalysts synthesized *ex situ*. (a)(b) Representative STEM images of PdSn/SiO₂. (c)(d) EDS elemental mapping of Pd and Sn on a PdSn nanoparticle and its surrounding in the marked region of (b). (e) HR-STEM image of a PdSn nanoparticle along the (100) direction and its corresponding crystal model. Scale bar: 0.5 nm. (f) PXRD of PdSn/SiO₂ formed *ex situ* via water and liquid nitrogen (LN₂) quench. (g) Pd 3d (top) and Sn 3d (bottom) XPS spectra of PdSn/SiO₂ formed *ex situ* via water quench.

Results and Discussion

The long-range-ordered structure of iNPs results in their thermodynamically favored formation and makes it easier to be characterized with tools such as PXRD, XAS, X-ray photoelectron spectroscopy (XPS), and high-resolution scanning transmission electron microscopy (STEM). The synthesis of bulk intermetallic compounds is relatively well guided by phase diagrams. Nanoparticles, on the contrary, exhibit distinct thermodynamic properties that often cannot be predicted from the bulk material. This constantly challenges the synthesis of intermetallic structures at the nanoscale. For example, previous work in our group studied the formation of PtSn and Pt₃Sn iNPs,^[13] where we found that PtSn iNPs readily form at 250 °C despite a eutectic point of 1268 °C on the Pt-Sn phase diagram.

With this impression, we investigated the synthesis of the PdSn phase by a pore-filling impregnation method with equal molars of Pd(II) and Sn(II) precursors. PXRD of the formed iNPs (Figure S1) after reduction at 300 °C clearly resembles the monoclinic Pd₃Sn₂ phase, despite the 1:1 Pd/Sn stoichiometry ratio. This result is consistent with previous observations.^[11d] To explore the possibility of forming an orthorhombic PdSn intermetallic phase, we performed temperature-dependent PXRD and XANES measurements under *in-situ* reduction conditions.

Initially, Pd nanoparticles (6.6 nm) are made as a platform for all later phase-transitioning experiments. Characterization of Pd/SiO₂ is shown in Figure S1-S2. After impregnating Sn(II) precursors, we pre-reduce the samples at 300 °C to form Pd₃Sn₂ nanoparticles to focus on any Pd₃Sn₂ to PdSn transition. When heated *in situ* to 600 °C, the sample with a 1:1 Pd/Sn stoichiometry ratio does not exhibit a clear phase transformation

(Figure S3). A K-type thermocouple is used during the experiment to monitor the temperature, and its diffraction peaks (Figure S4) in the obtained PXRD patterns should not be considered.

Interestingly, as shown in Figure 1a and Figure S5, with three equivalence of Sn to Pd in the sample, the PdSn phase starts to form at 400 °C. Further annealing at higher temperatures increased the PdSn component, and eventually, it achieved a pure PdSn phase at around 520 °C, which is confirmed by Rietveld quantitative analysis (Figure S6). We also note that an intermediate phase, Pd₂Sn, was observed during the heating process at scan #3, before the appearance of PdSn. We believe that Sn is not entirely reduced during the 300 °C pre-reduction because of its lower reduction potential than Pd, and thus creating a Pd-rich environment in the sample. Pd₂Sn is a known phase to form at appropriate Pd-rich stoichiometry,^[14] and it quickly transforms to PdSn when Sn is reduced at higher temperatures. These results indicate that the Pd/Sn ratio plays a significant role in forming the PdSn phase. In addition, PdSn slowly reverts to Pd₃Sn₂ once cooled down below 520 °C, which indicates the metastability of PdSn, a property that is not previously reported for bulk PdSn intermetallic and could be ascribed to the unique behavior of nano-sized intermetallic materials. Additional analysis of a Pd₃Sn control sample can be found in Figure S7.

To further understand the phase transition process, we also use *in-situ* X-ray absorption near edge structure (XANES) to monitor the formation of PdSn iNPs during the reduction of Sn precursor-loaded Pd/SiO₂. As shown in Figure 1c, the Pd/SiO₂ sample in the initial stage of the phase transition mostly resembles the Pd foil standard. Upon subsequent reduction of Sn(II), the characterization peak at ~24395 eV gradually shifts to

RESEARCH ARTICLE

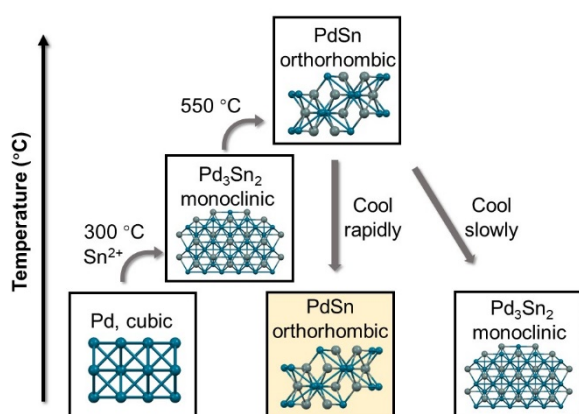


Figure 3. Schematic illustration of synthesizing PdSn iNPs and its metastability.

lower energy, indicating the emerging Pd₃Sn₂ and PdSn phase. For clarity, selected XANES scans representing the process are shown in Figure 1c, and the full data set can be found in Figure S8. A linear combination fitting of data (Figure 1d) shows that Pd-Sn alloying starts at around 200 °C, and Pd has been fully transitioned into Pd₃Sn₂ at around 300 °C, consistent with our *ex-situ* PXRD. Further increasing temperature facilitates the formation of the PdSn phase at above 360 °C. After the temperature reaches 550 °C, the sample is predominantly composed of the PdSn phase.

Furthermore, we have analyzed the Pd K-edge extended X-ray absorption fine structure (EXAFS) at key temperatures during the transformation under *in-situ* heating. See Table S1 and Figure S9-S10 for detailed fitting parameters. The change in the total coordination number (CN) of Pd is induced by the structural change during phase transition (Figure 1e). At 25 °C, the total CN is 12 as in Pd, and upon annealing to 300-350 °C, the total CN drops to 11, matching Pd₃Sn₂. Eventually, the total CN of Pd decreases to 6, indicating the formation of pure PdSn at >550 °C. Therefore, the XANES and EXAFS results are highly consistent with the *in-situ* PXRD study.

In addition, XANES analysis of Sn K-edge is used to determine the change in the chemical state of Sn. As shown in Figure 1f, the oxidation state of Sn obtained from XANES is around 3.2, likely as a result of oxidation of SnCl₂ in air. During the *in-situ* reduction, the oxidation state of Sn gradually drops until it reaches around 1.6 at 550-600 °C. Thus, we believe that the final PdSn nanocatalyst contains a mixture of Sn(II)/Sn(IV) and Sn(0) species, and we will further discuss it with XPS results later in the text. Additional EXAFS analysis of the Sn K-edge (Figure S10) shows the formation of Sn-Pd bonds during the *in-situ* reduction, supporting the formation of PdSn intermetallic phases, but a reliable quantitative analysis is challenging due to the complex chemical environment of different Sn species.

These *in-situ* characterization results enlightened us with the possibility to harvest the pure-phase PdSn *ex situ* through quenching. Such methods have been utilized in the synthetic routes of various materials.^[15] We anticipated that by heating the iNPs with a proper stoichiometry of Pd and Sn to above 550 °C and quench to room temperature rapidly, we could constrain atoms within the orthorhombic PdSn crystal structure at ambient condition. Among a range of quenching methods reported, we

found it most beneficial to use a cold water bath, which results in a pure PdSn phase (Figure 2f). A schematic demonstration of structural change during the synthesis of PdSn iNPs is shown in Figure 3. Rapid cooling is the key to obtain the PdSn orthorhombic phase iNPs. The as-obtained PdSn iNPs are characterized by electron microscopy. Initially, high-resolution high-angle annular dark-field (HAADF)-STEM and energy dispersive spectroscopy (EDS) mapping were performed to locate the excess Sn in the sample, as shown in Figure 2. Representative images of PdSn/SiO₂ show the formation of PdSn nanoparticles that exhibits two distinct regions, indicative of phase segregation within the nanoparticles. Their identities are further confirmed by EDS mapping (Figure 2c-d and Figure S11), where we observe both Pd and Sn signals in the brighter region and only Sn signals in the darker region. Meanwhile, there exist smaller (1-2 nm) clusters throughout the SiO₂ support, the identities of which are also discovered by EDS mapping to be Sn clusters. Therefore, we

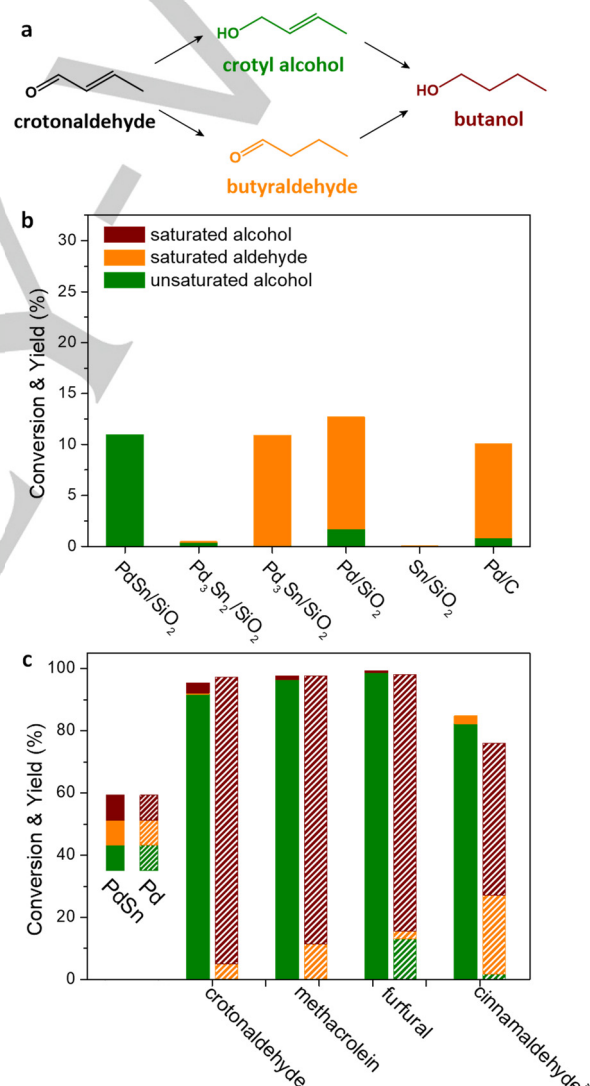


Figure 4. Catalysis results. (a) Schematic illustration of the reaction pathways in the hydrogenation of crotonaldehyde. (b) Product distribution for each catalyst at a conversion level of 10-15%.^[16] Reaction condition: 1.2 mmol crotonaldehyde, 1.2 mL H₂O, 8 bar H₂, 30 °C, 2 h. (c) Substrate scope study using different α,β -unsaturated aldehydes. Reaction condition: 1.2 mmol unsaturated aldehydes, 1.2 mL H₂O (*toluene for cinnamaldehyde), 8 bar H₂, 30 °C, 4 h (Pd catalysts) or 12 h (PdSn catalysts).

RESEARCH ARTICLE

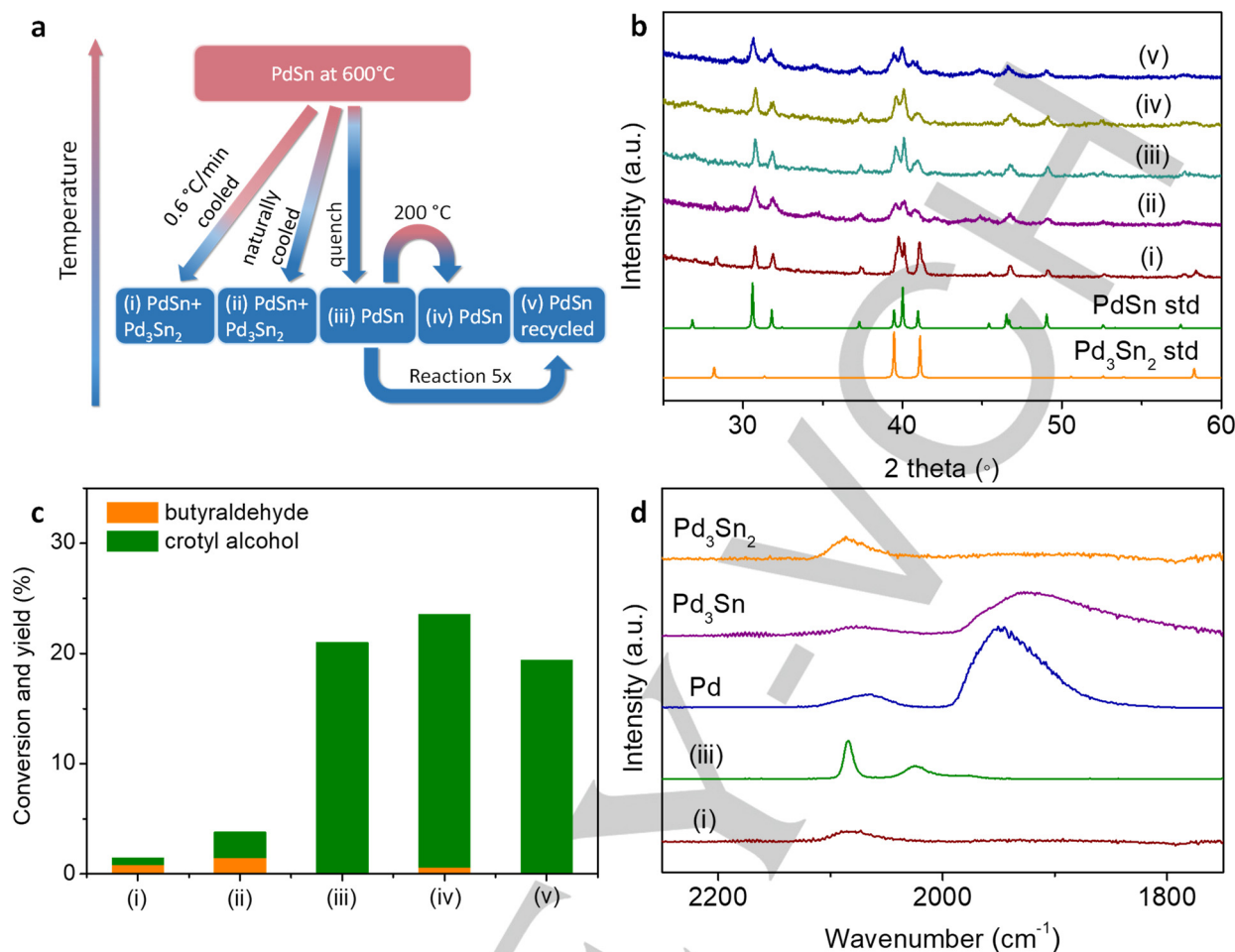


Figure 5. The structure-properties-relationship of the PdSn nanocatalyst. (a) Schematic illustration of the thermal treatments on PdSn nanocatalysts, (b) the corresponding PXRD patterns, (c) the corresponding catalytic behavior at reaction condition: 1.2 mmol crotonaldehyde, 1.2 mL H₂O, 8 bar H₂, 30 °C, 2 h. and (d) the CO-DRIFTS spectra, demonstrating key structural difference at catalyst surface induced by thermal treatments.

conclude that the excess Sn exists both as phase-segregated Sn crystals aside the PdSn iNPs, as well as small 1-2 nm Sn clusters distributed in the SiO₂ frame. An atomic-resolution image of a PdSn nanoparticle revealed a projection of the orthorhombic structure along the (100) direction, further confirming the identity of the PdSn phase. Figure 2e shows the crystal model of PdSn that matches the HAADF-STEM image. Inductively coupled plasma mass spectrometry (ICP-MS) confirms the loading of Pd and Sn in the catalyst to be 3.0 and 9.3 wt% (Table S2).

XPS measurement of the sample (Figure 2g) shows that in the Pd 3d spectrum, metallic Pd(0) peaks are dominant, featured by the characteristic peaks at 340.4 eV and 335.1 eV. While in the Sn 3d spectrum, deconvolution of the XPS peaks suggested 68% of the surface Sn species are in oxidized Sn(II) or Sn(IV) states. These values are highly consistent with the Sn K edge XANES fitting results mentioned earlier. Combining both the XANES and XPS results, we believe that the Sn(II)/Sn(IV) species are partially reduced during the reduction and form intermetallic PdSn, in which Sn species are metallic. The reduction of Sn is likely assisted with the presence of Pd crystal. We speculate that due to the catalyst being rich in Sn and the consumption of Pd to form PdSn iNPs, the majority of Sn remains as SnO_x species.^[17] We

should also note that XPS suggests the surface Pd and Sn composition, which cannot quantitatively represent the bulk PdSn intermetallic composition, considering the different sizes of the PdSn iNPs and the Sn domains/clusters revealed by TEM.

The catalytic properties of the PdSn iNPs were first examined on hydrogenation of crotonaldehyde (Figure 4a), a model reaction to study hydrogenation selectivity between C=O and C=C bonds. As shown in Figure 4b, the conversion of each catalyst is deliberately controlled at 10-15% (unless inactive) to fairly compare the selectivity of each catalyst.^[16] Additional catalysis results are presented in Figure S12, where catalysts' performance is compared with the same amount of Pd in each catalyst. Among various monometallic/bimetallic catalysts, PdSn has an outstanding selectivity of >99.9% to crotyl alcohol at a conversion of 11.0%. By extending the reaction time, we are also able to reach 95.4% in conversion while keeping a high (>96%) selectivity to crotyl alcohol (Figure 4c). In contrast, Pd and Pd₃Sn favor the formation of butyraldehyde, where the crotyl alcohol selectivity is merely 13.3% and 0.8%, respectively. Pd₃Sn₂/SiO₂ has a low activity toward this reaction, showing only a 0.5% conversion towards any product under the same reaction condition. This demonstrates that the catalytic behaviors are largely determined

RESEARCH ARTICLE

by the specific intermetallic structure. A commercial 5% Pd/C catalyst shows low selectivity (9.0%) to crotyl alcohol, similar to the Pd/SiO₂. A commercial 5% Pt/C catalyst shows no selectivity to crotyl alcohol and severe over-hydrogenation (Figure S12). These results are also comparable with previous literature.^[2a, 8, 18] Sn/SiO₂ shows no hydrogenation activity, ruling out any catalytic contribution from excess Sn in PdSn/SiO₂. However, potential indirect contribution from the SnO_x/PdSn interface cannot be excluded, as previous research reports such effects.^[19] Reaction yield to each product is calibrated (Figure S13) with gas chromatography (GC), and the carbon balance of each reaction is calculated to be within 100 ± 5% based on the calibration.

To show that the PdSn catalyst has a general high hydrogenation selectivity towards the C=O bond, we explore the substrate scope of the reaction with different α,β -unsaturated aldehydes, as shown in Figure 4c. The selectivities of Pd and PdSn catalysts are compared with crotonaldehyde, methacrolein, furfural, and cinnamaldehyde. The PdSn catalyst exhibits outstanding selectivity (96.2, 98.8, 99.5, and 97.3%, respectively) towards the C=O hydrogenation products in each reaction, outperforming the Pd monometallic catalysts that easily over-hydrogenate the substrate.

We then performed a variety of treatments on the PdSn nanocatalyst to establish the structure-properties relationship. As shown in Figure 5, one can correlate structural changes identified from PXRD and carbon monoxide diffuse reflectance infrared Fourier transform spectroscopy (CO-DRIFTS) study with catalytic performance. The PdSn/SiO₂ catalyst quenched from 600 °C to room temperature rapidly (iii in Figure 5) exhibits PdSn bulk phase and shows high C=O hydrogenation selectivity (>99.9%, 21% conversion) in crotonaldehyde hydrogenation; in contrary, PdSn/SiO₂ both slowly cooling down over a period of 16 h (i) and naturally cooling down (ii) show mixed phases of Pd₃Sn₂ and PdSn from the PXRD patterns in Figure 5b. Such mixed-phase catalysts result in low activity in crotonaldehyde hydrogenation (2.2% and 5.2% conversion, respectively), behaving similar to pure phase intermetallic Pd₃Sn₂.

To investigate the surface structural change, we use CO-DRIFTS to characterize these samples (Figure 5d). Monometallic Pd catalyst, as a reference, shows its characteristic atop CO adsorption peak at 2068 cm⁻¹ and bridged CO adsorption peak at 1950 cm⁻¹.^[20] Pd₃Sn₂ behaves similarly as Pd, showing a larger bridged than atop CO adsorption peak, which may explain their similarity in catalytic behavior. As the Pd sites are diluted by Sn atoms in Pd₃Sn₂, the bridged CO adsorption peak disappears due to a lack of neighbored Pd sites.^[21] Interestingly, the quenched PdSn nanocatalyst shows a strong atop CO adsorption at 2083 cm⁻¹ and a weak but unique peak at 2030 cm⁻¹. Our density functional theory (DFT) calculations of the vibrational frequencies of CO adsorbed on PdSn(012) suggest the vibration at 2083 and 2030 cm⁻¹ can be assigned to atop CO adsorption and a CO bridged between two surface Pd atoms (see detailed discussion in Figure S15). On the contrary, the slowly cooled PdSn catalyst shows a very similar CO adsorption peak with the Pd₃Sn₂ sample. Therefore, we believe that even though the reversion of the slowly/naturally cooled PdSn iNPs to Pd₃Sn₂ phase does not complete through the whole nanoparticle, the structural change likely starts at the catalyst surface where the energy barrier for reconstruction is the lowest. The resulting catalysts are most likely

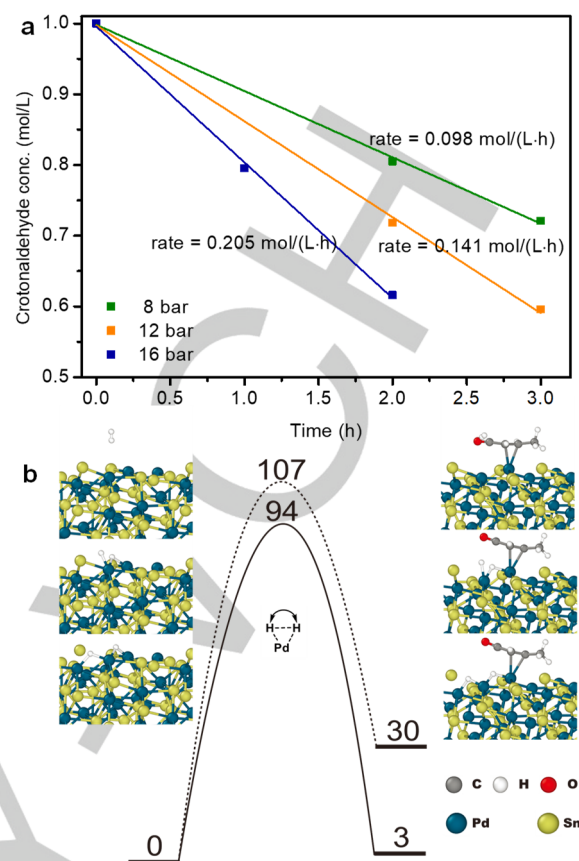


Figure 6. H₂ adsorption behavior over PdSn nanocatalyst. (a) Initial rate of crotonaldehyde hydrogenation measured at different H₂ pressure, showing an order of approximately 1 in H₂ for crotonaldehyde hydrogenation over PdSn. (b) Schematic illustration of the calculated H₂ dissociation process and energy barrier, with and without the presence of adsorbed crotonaldehyde molecules. The unit is kJ/mol.

possessing a prevailing Pd₃Sn₂ surface, therefore behave like Pd₃Sn₂ in CO-DRIFTS and show low activity in crotonaldehyde hydrogenation.

Besides, a 200 °C treatment (4 h) is also performed on the quenched PdSn/SiO₂ catalyst (iv), and it shows comparable PXRD pattern and catalytic performance (97.8% selectivity, 24.1% conversion) after the treatment. This comparison indicates that the PdSn iNPs do not convert to Pd₃Sn₂ at 200 °C in 4 h and are thus stable at our reaction temperature (30 °C). This result also demonstrates the possibility of applying this catalyst to other reactions that require moderate temperature. A 5-times recycled catalyst also confirms the catalyst stability, showing comparable PXRD pattern (Figure 5b), XPS spectra (Figure S14), and catalytic performance (>99.9% selectivity, 19.7% conversion) as the fresh catalyst.^[22]

Further understanding of such high C=O selectivity in crotonaldehyde hydrogenation can be learned by measuring reaction orders over the PdSn catalyst. As shown in Figure 6a and Figure S16, the reaction order of crotonaldehyde is observed to be approximately zero, and the reaction order of H₂ pressure is approximately 1. Those reaction orders suggest that either the surface is covered by crotonaldehyde or crotonaldehyde is not involved in the rate-determining step. To explain the reaction

RESEARCH ARTICLE

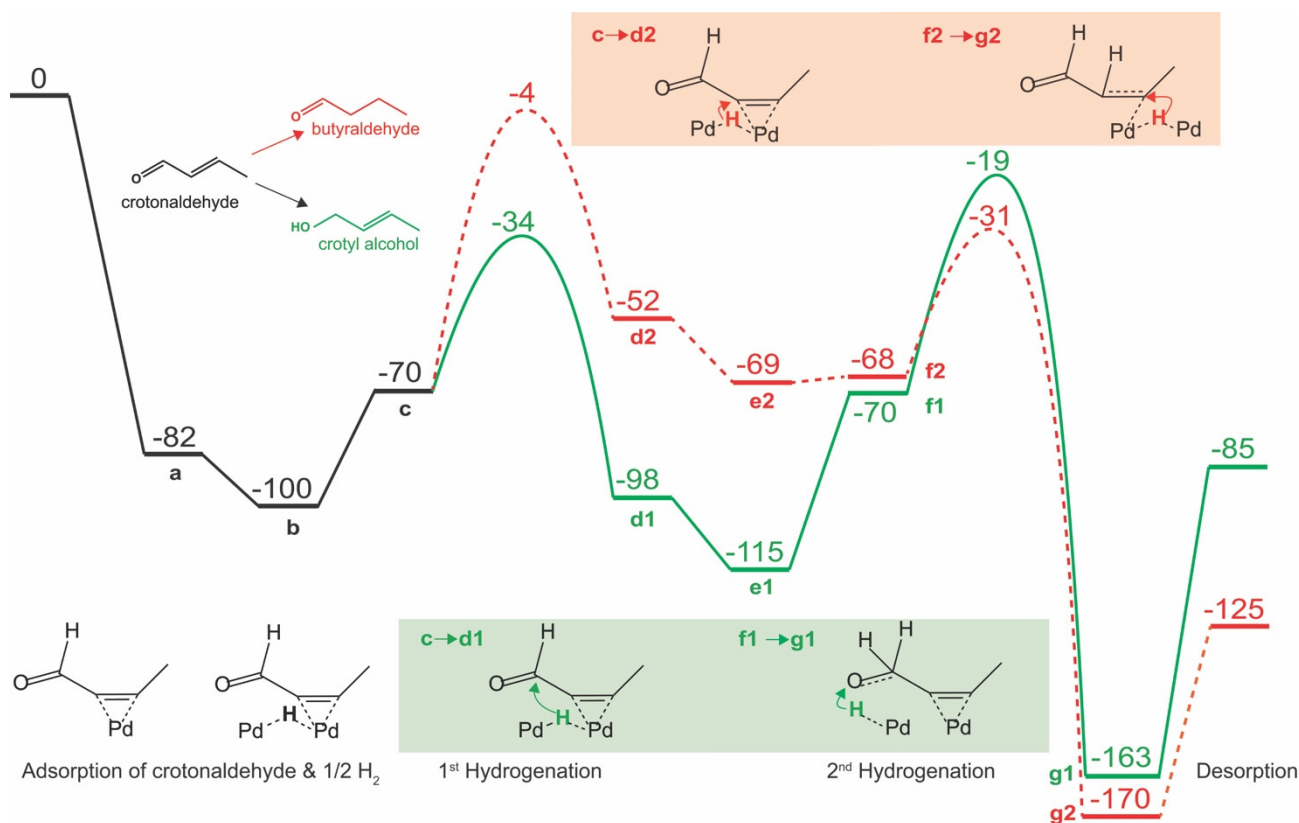


Figure 7. DFT-calculated reaction mechanism for crotonaldehyde hydrogenation over PdSn (012) surface. The path for hydrogenation of the C=C and C=O bond is colored red and green, respectively. The insets show the schematics for the elementary steps, crotonaldehyde and H₂ adsorption, hydrogenation, and desorption. The unit is kJ/mol. The atomic structures of the intermediates and transition states are shown in the supplementary information.

order and the observed high selectivity, we conducted DFT calculations.

The hydrogen dissociation (Figure 6b) is initiated via adsorption of dihydrogen on the Pd-Sn surface. DFT calculation shows that the dissociation proceeds with an activation barrier of 94 kJ/mol. In the presence of crotonaldehyde on the surface, the dissociation barrier of the dihydrogen increases to 107 kJ/mol. To further understand the H₂ dissociation behavior, we conducted the crotonaldehyde hydrogenation using D₂O as the solvent. The reaction mixtures were analyzed by solution NMR (Figure S17), showing no formation of C-D bonds in the methylene of crotyl alcohol, confirmed by GC-MS (Figure S18). GC-MS results also show partial H-D exchange on the -OH group of crotyl alcohol, which readily occurs in the presence of the D₂O solvent. The *in-situ* NMR experiment using D₂O solvent and 6 bar H₂ also shows the absence of HD formation even after 24 h at 60 °C (Figure S19). However, it is commonly observed that Pd nanoparticles can catalyze the rapid H-D exchange between H₂ and D₂O, readily leading to the deuterium incorporation in the hydrogenation products.^[23] This divergent behavior of PdSn versus Pd suggests that the activation of H₂ by PdSn is much slower. Thus, adsorbed hydrogen has a relatively transient lifetime, indicating a high dissociation barrier.

Figure 7 shows the calculated energy profile to compare the two competing pathways, which are hydrogenation of the C=O bonds of crotonaldehyde to form crotyl alcohol and the C=C bonds to form butyraldehyde. The initial step is the adsorption of reactants (Figure S20 and S21) on a clean PdSn surface. Note the adsorption of crotonaldehyde (a in Figure 7) is much stronger

than hydrogen (b in Figure 7), indicating the PdSn surface is likely covered by crotonaldehyde. The second step is the hydrogen migration (b-c in Figure 7) to a Pd-Pd bridge site in the proximity of crotonaldehyde with an energy cost of 30 kJ/mol.

There are two elementary steps for hydrogenation of the C=O and C=C double bonds; only the ones with the lowest activation barrier are included in Figure 7, while the alternate sequences for hydrogenation are included in the supplementary information (Figure S21-25). To hydrogenate the C=C bond (c-d2 in Figure 7), the intrinsic barrier for the first hydrogenation is 66 kJ/mol, followed by the second barrier of 37 kJ/mol to hydrogenate the other carbon in the C=C bond to form butyraldehyde, leading to an overall barrier of 78 kJ/mol with respect to the gas phase H₂. The formation of crotyl alcohol by hydrogenation of the C=O bond is relatively easier; the overall barrier is 63 kJ/mol.

It appears that desorption of butyraldehyde or crotyl alcohol should not limit the reaction kinetics because the energy cost for desorption of butyraldehyde and crotyl alcohol is 45 and 78 kJ/mol, respectively. If the entropy gain upon desorption is included, the desorption energy can be further reduced (see supplementary information). The broken ensemble of surface Pd reduces the binding between the surface and the butyraldehyde and crotyl alcohol, the latter of which can thus desorb without further hydrogenation to produce butanol.

The activation barrier to hydrogenate the C=O and C=C double bonds is considerably smaller than the aforementioned dissociation barrier of hydrogen over the Pd-Sn surface, indicating the hydrogenation reaction is limited by the activation of the H₂ on the surface. This is consistent with our experimental

RESEARCH ARTICLE

result using D₂O as the reaction solvent. To further illustrate this conclusion, we performed a kinetic analysis based on the Langmuir–Hinshelwood mechanism. We considered both a two-site model in which H and crotonaldehyde do not compete for sites and a one-site model where they do compete. This analysis is similar to what we recently performed for hydrogenation of furfural,^[24] which also includes a conjugated C=C and C=O bonds. The kinetics analysis (Table S4), combined with our DFT calculation discussed above, suggests the reaction is limited by H₂ dissociation; this agrees with the experimentally measured 1st order of reaction rate with respect to H₂ pressure. Interestingly, though it does not determine the rate, the reaction selectivity is indeed determined by hydrogenation of the C=C and C=O bonds; the higher overall barrier for hydrogenation of the C=C than C=O bonds thus explains the high selectivity to the unsaturated alcohol.

Conclusion

In summary, we demonstrated the use of *in-situ* techniques that enables the synthesis of intermetallic PdSn nanocatalysts. Both *in-situ* PXRD and XANES studies confirm that a temperature above 550 °C is necessary to obtain the pure PdSn phase, while Pd₂Sn and Pd₃Sn₂ intermediates present at lower temperatures. In addition, the PdSn phase reverts to a thermodynamically preferred Pd₃Sn₂ phase over a slow cooling process, but an efficient quenching method harvests the PdSn nanocatalyst successfully. We believe that this surface-specific phase transition appears uniquely on nanomaterials. As for bulk material, such transition would be masked by the dominant bulk phase in PXRD measurements. This could nurture future studies about distinct behaviors of nanomaterials. Applied to the hydrogenation of crotonaldehyde as well as other α,β -unsaturated aldehydes, the PdSn nanocatalyst exhibits excellent C=O hydrogenation selectivity. Other catalysts, such as Pd, Pd₃Sn, and Pd₃Sn₂, show either poor selectivity or low activity. To the best of our knowledge, this is the highest selectivity reported for this reaction with Pd-based catalysts. Further studies demonstrate the significance of efficient quenching in obtaining high activity and selectivity: a Pd₃Sn₂-surfaced catalyst obtained after a natural cooling process results in impaired catalytic selectivity and similar activity to pure phase Pd₃Sn₂. CO-DRIFTS studies indicate that the reversion from PdSn to Pd₃Sn₂ likely started at the surface of the catalyst. Isotope-labelling studies show a short lifetime of adsorbed hydrogen, indicating a high H₂ dissociation barrier. DFT calculations suggest an energetic preference in the hydrogenation of the C=O bonds over PdSn surface and determine the rate-limiting step of the catalytic reaction to be H₂ dissociation on the PdSn surface.

Acknowledgements

This work is partially supported by NSF grant CHE-1808239. The computations were performed at the OU Supercomputing Center for Education & Research and the National Energy Research Scientific Computing Center (NERSC), a U.S. Department of Energy Office of Science User Facility, and were supported by the U.S. Department of Energy, Basic Energy Sciences (Grant DE-SC0018284). This work was partially supported by the US Department of Energy, Basic Energy Science (Grant No. DE-

SC0013897) for Early Career Research. This research used resources of the Advanced Photon Source, a U.S. Department of Energy (DOE) Office of Science User Facility operated for the DOE Office of Science by Argonne National Laboratory under Contract No. DE-AC02-06CH11357. L.Q. was supported by the U.S. Department of Energy (DOE), Office of Basic Energy Sciences, Division of Chemical Sciences, Geosciences, and Biosciences through the Ames Laboratory Catalysis program. The Ames Laboratory is operated for the U.S. DOE by Iowa State University under Contract No. DE - AC02 - 07CH11358. We thank Matt Besser for the use of the X-ray diffractometer. We thank Taehoon Kim for assistance in STEM imaging at Ames Laboratory Sensitive Instrument Facility. We are grateful to Yujia Ding and Chengjun Sun for their help during the XANES measurement at stations 10-ID and 20-BM-B of Advanced Photon Source.

Keywords: intermetallic phases • metastable compounds • α,β -unsaturated aldehydes • heterogeneous catalysis • nanoparticles

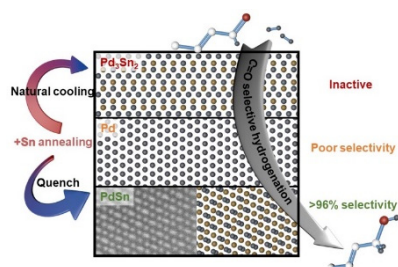
- [1] a) P. Mäki-Arvela, J. Hájek, T. Salmi, D. Y. Murzin, *Appl. Catal. A* **2005**, 292, 1-49; b) P. Gallezot, D. Richard, *Cat. Rev.* **1998**, 40, 81-126.
- [2] a) N. Iwasa, M. Takizawa, M. Arai, *Appl. Catal. A* **2005**, 283, 255-263; b) P. Aich, H. Wei, B. Basan, A. J. Kropf, N. M. Schweitzer, C. L. Marshall, J. T. Miller, R. Meyer, *J. Phys. Chem. A* **2015**, 119, 18140-18148; c) A. S. Nagpure, L. Gurrula, P. Gogoi, S. V. Chilukuri, *RSC Adv.* **2016**, 6, 44333-44340; d) S. T. Marshall, M. O'Brien, B. Oetter, A. Corpuz, R. M. Richards, D. K. Schwartz, J. W. Medlin, *Nat. Mater.* **2010**, 9, 853-858.
- [3] M. Tamura, K. Tokonami, Y. Nakagawa, K. Tomishige, *ACS Catal.* **2016**, 6, 3600-3609.
- [4] a) G. C. Torres, S. D. Ledesma, E. L. Jablonski, S. R. de Miguel, O. A. Saelza, *Catal. Today* **1999**, 48, 65-72; b) S. Recchia, C. Dossi, N. Poli, A. Fusi, L. Sordelli, R. Psaro, *J. Catal.* **1999**, 184, 1-4; c) L. Sordelli, R. Psaro, G. Vlaic, A. Cepparo, S. Recchia, C. Dossi, A. Fusi, R. Zanon, *J. Catal.* **1999**, 182, 186-198; d) E. Galloway, M. Armbruster, K. Kovnir, M. S. Tikhov, R. M. Lambert, *J. Catal.* **2009**, 261, 60-65.
- [5] R. V. Maligal-Ganesh, C. X. Xiao, T. W. Goh, L. L. Wang, J. Gustafson, Y. C. Pei, Z. Y. Qi, D. D. Johnson, S. R. Zhang, F. Tao, W. Y. Huang, *ACS Catal.* **2016**, 6, 1754-1763.
- [6] S. S. Ashour, J. E. Bailie, C. H. Rochester, J. Thomson, G. J. Hutchings, *J. Mol. Catal. A: Chem.* **1997**, 123, 65-74.
- [7] B. Chen, F. Li, Z. Huang, G. Yuan, *Appl. Catal. A* **2015**, 500, 23-29.
- [8] B. C. Campo, M. A. Volpe, C. E. Gigola, *Ind. Eng. Chem. Res.* **2009**, 48, 10234-10239.
- [9] a) A. Vicente, G. Lafaye, C. Especel, P. Marécot, C. T. Williams, *J. Catal.* **2011**, 283, 133-142; b) J. Zhao, X. Xu, X. Li, J. Wang, *Catal. Commun.* **2014**, 43, 102-106.
- [10] a) A. Brouzgou, S. Song, P. Tsiakaras, *Appl. Catal. B* **2014**, 158-159, 209-216; b) A. Garron, K. Lazar, F. Epron, *Appl. Catal. B* **2005**, 59, 57-69; c) L. Lemaignen, C. Tong, V. Begon, R. Burch, D. Chadwick, *Catal. Today* **2002**, 75, 43-48.
- [11] a) H. Lorenz, C. Rameshan, T. Bielz, N. Memmel, W. Stadlmayr, L. Mayr, Q. Zhao, S. Soisuwan, B. Klotzer, S. Penner, *ChemCatChem* **2013**, 5, 1273-1285; b) H. Lorenz, Q. A. Zhao, S. Turner, O. I. Lebedev, G. Van Tendeloo, B. Klotzer, C. Rameshan, K. Pfaller, J. Konzett, S. Penner, *Appl. Catal. A* **2010**, 381, 242-252; c) J. Arana, P. R. de la Piscina, J. Llorca, J. Sales, N. Homs, J. L. G. Fierro, *Chem. Mater.* **1998**, 10, 1333-1342; d) S. Furukawa, M. Endo, T. Komatsu, *ACS Catal.* **2014**, 4, 3533-3542.
- [12] N. H. Chou, R. E. Schaak, *J. Am. Chem. Soc.* **2007**, 129, 7339-7345.
- [13] a) M. Chen, Y. Han, T. W. Goh, R. Sun, R. V. Maligal-Ganesh, Y. Pei, C.-K. Tsung, J. W. Evans, W. Huang, *Nanoscale* **2019**, 11, 5336-5345; b) T. Ma, S. Wang, M. Chen, R. V. Maligal-Ganesh, L.-L. Wang, D. D. Johnson, M. J. Kramer, W. Huang, L. Zhou, *Chem* **2019**, 5, 1235-1247; c) W. Zhao Evan, R. Maligal-Ganesh, C. Xiao, T. W. Goh, Z. Qi, Y. Pei, E. Hagelin-Weaver Helena, W. Huang, R. Bowers Clifford, *Angew. Chem.* **2017**, 129, 3983-3987.
- [14] K. Page, C. S. Schade, J. Zhang, P. J. Chupas, K. W. Chapman, T. Proffen, A. K. Cheetham, R. Seshadri, *Mater. Res. Bull.* **2007**, 42, 1969-1975.
- [15] a) S. Akbulut, Y. Ocak, N. Maraşlı, K. Keşlioğlu, U. Böyük, E. Çadırılı, H. Kaya, *Mater. Charact.* **2008**, 59, 1101-1110; b) J. A. Steele, H. Jin, I. D. Dvoglgiuk, R. F. Berger, T. Braeckevelt, H. Yuan, C. Martin, E. Solano, K. Lejaeghere, S. M. J. Rogge, C. Notebaert, W. Vandezande, K. P. F. Janssen, B. Goderis, E. Debroye, Y.-K. Wang, Y. Dong, D. Ma, M. Saidaminov, H. Tan, Z. Lu, V. Dyadkin, D. Chernyshov, V. Van

RESEARCH ARTICLE

- Speybroeck, E. H. Sargent, J. Hofkens, M. B. J. Roeffaers, *Science* **2019**, eaax3878; c) M. J. Costello, J. M. Corless, *J. Microsc.* **1978**, *112*, 17-37.
- [16] F. Schüth, M. D. Ward, J. M. Buriak, *Chem. Mater.* **2018**, *30*, 3599-3600.
- [17] J. Yang, K. Hidajat, S. Kawi, *J. Mater. Chem.* **2009**, *19*, 292-298.
- [18] M. A. Vannice, B. Sen, *J. Catal.* **1989**, *115*, 65-78.
- [19] W.-P. Zhou, W. An, D. Su, R. Palomino, P. Liu, M. G. White, R. R. Adzic, *J. Phys. Chem. Lett.* **2012**, *3*, 3286-3290.
- [20] a) I. Jbir, J. Couble, S. Khaddar-Zine, Z. Ksibi, F. Meunier, D. Bianchi, *ACS Catal.* **2016**, *6*, 2545-2558; b) M. Liu, W. Tang, Y. Xu, H. Yu, H. Yin, S. Zhao, S. Zhou, *Appl. Catal. A* **2018**, *549*, 273-279.
- [21] R. Manrique, J. Rodríguez-Pereira, S. A. Rincón-Ortiz, J. J. Bravo-Suárez, V. G. Baldovino-Medrano, R. Jiménez, A. Karelavic, *Catal. Sci. Technol.* **2020**, *10*, 6644-6658.
- [22] C. W. Jones, *Top. Catal.* **2010**, *53*, 942-952.
- [23] a) T. Kurita, F. Aoki, T. Mizumoto, T. Maejima, H. Esaki, T. Maegawa, Y. Monguchi, H. Sajiki, *Chem. Eur. J.* **2008**, *14*, 3371-3379; b) X. C. Guo, R. J. Madix, *J. Catal.* **1995**, *155*, 336-344.
- [24] Z. Zhao, R. Bababrik, W. H. Xue, Y. P. Li, N. M. Briggs, D. T. Nguyen, U. Nguyen, S. P. Crossley, S. W. Wang, B. Wang, D. E. Resasco, *Nat. Catal.* **2019**, *2*, 431-436.

RESEARCH ARTICLE

Entry for the Table of Contents



Metastable PdSn intermetallic nanoparticles are made through a rapid quenching method, inspired by *in-situ* characterization results. PdSn shows unprecedented high hydrogenation selectivity of C=O over C=C bonds in α,β -unsaturated aldehydes.